
This is an electronic reprint of the original article.
This reprint may differ from the original in pagination and typographic detail.

Mousavi, Mahdi; Bernad, Andreu; Alopaeus, Ville

Modeling oil/water emulsion separation in batch systems with population balances in the presence of surfactant

Published in:
Chemical Engineering Science

DOI:
[10.1016/j.ces.2024.120558](https://doi.org/10.1016/j.ces.2024.120558)

Published: 05/12/2024

Document Version
Publisher's PDF, also known as Version of record

Published under the following license:
CC BY

Please cite the original version:
Mousavi, M., Bernad, A., & Alopaeus, V. (2024). Modeling oil/water emulsion separation in batch systems with population balances in the presence of surfactant. *Chemical Engineering Science*, 300, Article 120558.
<https://doi.org/10.1016/j.ces.2024.120558>

This material is protected by copyright and other intellectual property rights, and duplication or sale of all or part of any of the repository collections is not permitted, except that material may be duplicated by you for your research use or educational purposes in electronic or print form. You must obtain permission for any other use. Electronic or print copies may not be offered, whether for sale or otherwise to anyone who is not an authorised user.



Modeling oil/water emulsion separation in batch systems with population balances in the presence of surfactant

Mahdi Mousavi^{*}, Andreu Bernad, Ville Alopaeus

Aalto University, School of Chemical Engineering, Department of Chemical and Metallurgical Engineering, P.O. Box 11000, FI-00076 Aalto, Finland

ARTICLE INFO

Keywords:

Batch Separation
Coalescence
Dispersion
Oil Water Emulsion
Creaming
Sedimentation

ABSTRACT

This study introduces a simplified model for batch gravitational separation of liquid–liquid dispersions, integrating a decantation model with a high order moment conserving method of classes in population balances (PBM-HMMC). The proposed model incorporates the dynamics of surfactants and their effect on droplet size distribution, emphasizing the crucial influence of surfactants on emulsion stability. Notably, while extensive literature exists on predicting interphases in batch separation with surfactants, the application of population balance methods to predict droplet size distribution evolution is scarcely addressed, which is a primary focus of this work. The model's accuracy is verified through comparison with independent experimental data, confirming its practical relevance. Furthermore, the research explores the impact of various parameters, including emulsion height, surfactant concentration and type, and droplet size distribution, on the separation process.

1. Introduction

Separating liquid–liquid dispersions is a widespread issue in industries like petroleum, petrochemical, hydrometallurgy, nuclear fuel processing, and chemicals (Ahmad and Nolle, 2021; Hidayah and Abidin, 2018). This separation is typically done using gravity settlers and centrifuges, designed from expensive pilot plant tests. Researchers have tried to grasp this process by observing droplet sedimentation, creaming, and coalescence in small-scale, cost-effective batch separators. Predicting the system parameters like residence time and maximum droplet size in liquid–liquid phase separation is crucial for the efficient design and operation of real-size decanters (Stewart and Arnold, 2008). Accurate predictions of residence time ensure that the mixture has sufficient time to separate into distinct phases, optimizing the separation process. An underestimation can lead to incomplete separation, affecting product quality and efficiency, while an overestimation may result in oversized equipment or increased energy consumption (Hooper et al., 1979; Mousavi et al., 2021). Due to the complexity of physical experiments, employing mathematical models and simulations is becoming a preferred approach to study and design batch settlers.

Fig. 1 illustrates a typical batch gravity settler operation, identifying four key areas during phase separation: an aqueous phase, an organic phase, a dense-packed zone, and a creaming/sedimentation zone. At the start (time $t = 0$), either sedimentation or creaming occurs, depending

on the density of the dispersed phase relative to the continuous phase. Depending on the emulsion type (water in oil or oil in water), either sedimentation or creaming occurs. These two mechanisms in liquid–liquid decantation can happen simultaneously, but often one is more dominant, influenced by the densities of the liquids (Hooper et al., 1979). Sedimentation is a process that occurs when the dispersed phase has a higher density than the continuous phase, and due to gravity, droplets move downward in the continuous phase. Creaming is also a gravity-driven process, and it involves the upward migration of droplets in the dispersion layer because the dispersed phase is lighter than the continuous phase. In Fig. 1 the light phase is dispersed; therefore, this work will use the term 'creaming' for clarity. Initially, droplets grow through droplet–droplet coalescence in the dispersion zone. If this growth is faster than droplet–interface coalescence (droplets merging with their homophase), they accumulate in the dense-packed zone and later merge with their homophase (Thaker and Buwa, 2019). Therefore, the droplets at the interface end up larger than those originally formed. At a so-called inflection point ($t = t_i$), where h_d equals h_s , the creaming process concludes, resulting in three distinct layers: the aqueous phase, the organic phase, and the dense-packed zone. Eventually, after a certain period ($t = t_f$), all droplets vanish, leaving a distinct interface (Henschke et al., 2002).

Many authors have introduced sedimentation-based models to understand the mechanism of phase separation in emulsions (Henschke et al., 2002; Jeelani and Hartland, 1986; Bhardwaj and Hartland, 1994;

^{*} Corresponding author.

E-mail address: mahdi.mousavi@aalto.fi (M. Mousavi).

Nomenclature

A	Cross-sectional area of the vessel, m^2	t	Time (s), s
a_i	Surface area of a droplet in category i , m^2	U_t	Terminal velocity (Stokes law), m/s
B_c	Birth term of population due to droplet–droplet coalescence, –	V_0	Initial volume of the dispersion, m^3
c	concentration of surfactant in the bulk phase, mol/m^3	V_o	Organic phase volume, m^3
C_1	Empirical parameter for interfacial coalescence frequency correlation, –	V_t	Total volume, m^3
D	Mean droplet diameter at time t , m	V_w	Aqueous phase volume, m^3
D_0	Initial average droplet diameter, m	Y	Population number density, –
D_c	Death term of population due to droplet–droplet coalescence, –	α	Average volume fraction of dispersed phase, <i>fraction</i>
g	Acceleration due to gravity (approximately 9.81), m/s^2	α_0	Initial dispersed phase fraction, <i>fraction</i>
H_0	Initial height of the dispersion, m	α_d	Maximum dispersed phase fraction in dense-packed zone, <i>fraction</i>
h_c	Height of the coalescence interface, m	β	Diminishing volume fraction of the dispersion due to interfacial coalescence, <i>fraction</i>
h_d	Height of the dense-packed zone interface	Γ	Surface concentration, mol/m^2
H_d	Height of dispersion, m	Γ_m	Maximum surface concentration, mol/m^2
h_s	Height of the creaming interface, m	$\Delta\rho$	Density difference between the dispersed and continuous phases, kg/m^3
K_L	Langmuir equilibrium adsorption constant, m^3/mol	ϵ	Turbulence energy dissipation rate, m^2/s^3
L_i, L_j	Representative of i^{th} and j^{th} diameter groups, m	μ_c	Dynamic viscosity of continuous phase, $Pa.s$
n	Number of surfactant moles, mol	ξ	Ratio of droplets leaving the dispersion layer to previous time step, <i>fraction</i>
n_{RZ}	Richardson and Zaki coefficient. Equal to 5.1 in this work, –	σ	Interfacial tension between oil and water, N/m
r_{bc}	Rate of binary coalescence, $1/s$	ρ_c	Density of continuous phase, kg/m^3
S	Sink term of population balance due to droplet-interface coalescence, –	ρ_d	Density of dispersed phase, kg/m^3
		φ_c	Coalescence frequency, –
		φ_e	Coalescence efficiency, –

Phase Separation Behavior

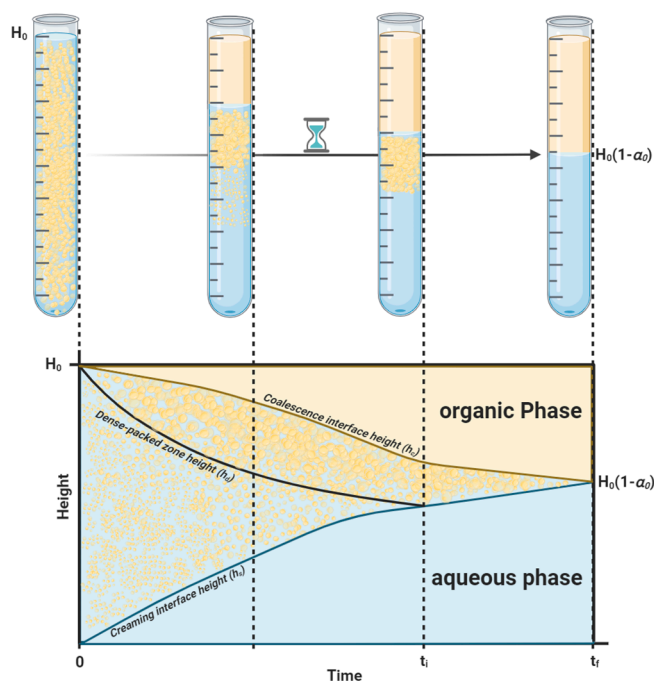


Fig. 1. The separation efficiency of oil in water emulsion in the batch separator is illustrated in terms of creaming, dense-packed zone, and coalescing interface height over time.

Jeelani et al., 1999; Aleem, 2021; Khan, 2019; Grimes, 2012). Stokes (1851) was the first to analyze sedimentation in significant depth, which led to a formulation of the equation for the settling velocity of a single hard sphere, known as Stoke's law (Stokes, 1851). Nadiv and Semiat (1995) conducted experimental research to examine the influence of mixing conditions and dispersion height on the separation of batch dispersions using two different settler diameters (Nadiv and Semiat, 1995). However, they did not deliberately alter the dispersion holdup. Their model for sedimentation was built upon the analysis by Aris and Amundson (1973) concerning batch precipitation of solid suspensions (Schneider et al., 1973). To describe the coalescence profile, an empirical formula was employed. Their model incorporated four adjustable parameters that must be identified through experimental sedimentation and coalescence profiles. Jeelani and Hartland have adapted the Stokes law and the incorporation of the physical and chemical properties of droplets into sedimentation (Jeelani and Hartland, 1986). The model suggested by Jeelani and Hartland requires prior knowledge of the interfacial coalescence timeframe and initial droplet size (Jeelani and Hartland, 1998). In addition, they provide a formula for determining the initial droplet diameter based on the initial sedimentation velocity. As Noik et al. (2013) reported, coalescence happens when two droplets approach and collide (droplet–droplet coalescence) or when a droplet collides into its homophase (Noik et al., 2013). In their study, a model, including this coalescence behavior, is developed to predict the settling time of batch separators. However, it is essential to note that the model does not directly account for the effect of additives like surfactant concentration on sedimentation and coalescence behavior. It should be highlighted that their model utilized a collision efficiency coefficient, as the primary empirical parameter. This parameter is predominantly influenced by the physicochemical characteristics of the water–oil interfacial film, with factors such as oil composition and the presence of additives like demulsifiers playing significant roles.

Surfactants and their nature can significantly influence the liquid–liquid phase separation due to their effects on emulsion behavior and separation efficiency (Deng, 2002; Haegel, 2009; Hassanpour, 2018).

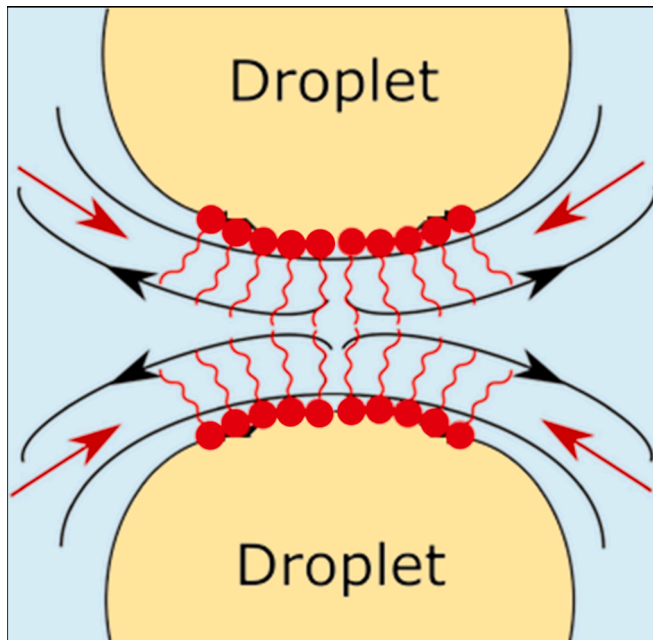


Fig. 2. The role of surfactant molecules (red circles with tails) in stabilizing droplets and inhibiting coalescence. The surfactants adsorb at the droplet interfaces, forming a barrier that repels approaching droplets and prevents them from merging.

Surfactants can thermodynamically be stable and thus more detrimental in the decantation process (Wang et al., 2012). As it is depicted in Fig. 2, surfactants stabilize emulsions by adsorbing at the oil–water interface and forming a barrier around droplets, preventing them from merging easily. They can change the size distribution of droplets within the emulsion by hindering the droplet–droplet coalescence (Alopaus, 2022). The presence of surfactants often results in more stable emulsions, which can be challenging to separate and it directly influences the separation process’s efficiency (Aleem, 2021).

The study of droplet interactions leads to a diverse range of droplet sizes. Several researchers have used population balances to model the droplet size distribution (Grimes, 2012; Wang and Davis, 1995; Ruiz and Padilla, 1996; Gomes et al., 2007; Cunha, 2008). The population balances, which depend on experimental data, describe the collective behavior of droplets without focusing on each one individually. Alopaus (2022) expanded a material balance approach for population balances, focusing on the interface material balance of surfactants in liquid–liquid systems (Alopaus, 2022). The High Order Moment Conserving Method of Classes (HMMC) serves as a method for evaluating droplet size distributions in the droplet phase (Buffo and Alopaus, 2017). By integrating this model with a material balance and relevant physical closures, it can effectively predict the behavior of liquid–liquid dispersions (Alopaus, 2022). This streamlined approach offers a more modest yet adequately detailed perspective on the model’s capabilities.

This work aims to model the liquid–liquid phase separation and predict the surfactant’s effect on oil stabilization in water emulsion. In this study, a mathematical model based on Stokes law is developed to examine the separation profile and droplet–interface coalescence. The surfactant effect is included in the model through a population balance (HMMC) with appropriate droplet coalescence closures, predicting the droplet size distribution evolution over time. While there is a significant amount of literature on the prediction of interphases in batch separation in the presence of surfactants, literature on applying population balance approaches to predict drop size distribution evolution is limited. This gap is one of the main objectives of the present work and is clearly emphasized in our model. Indeed, to effectively predict the phase separation process, both droplet–droplet and droplet–interface coalescence

processes must be accounted for in these models. The proposed model has been validated against experimental data from controlled tests, ensuring its accuracy in predicting the phase separation process. Additionally, an analysis was conducted to assess the effects of the number of preserved moments and categories. Subsequently, the model’s behavior is analyzed in the presence of a hypothetical surfactant, considering variations in concentration and type.

The structure of the paper is the following: The proposed mathematical model is presented in Section 2. In Section 3, the validation and verification of the model, and numerical examples, are presented. Section 4 offers the conclusions.

2. Model development

Droplet–droplet and droplet–interface coalescence rates are functions of various factors, including the initial droplet size distribution (DSD), inlet dispersed phase volume fraction, and the physical properties of the liquids, such as densities, viscosities, and interfacial tension. Equipment geometry, such as the settling area and equipment internals, also comes into play. Hence, understanding these parameters’ role on phase separation rate is critical. Droplet–droplet coalescence and droplet–interface coalescence are depicted in Fig. 3.

Fig. 4 depicts the decantation process in a separation vessel, showing four layers initially: an aqueous phase, an organic phase, a dense-packed zone, and a creaming zone. The process is split into two stages: before and after the inflection point (t_i). Prior to t_i , the creaming zone’s height (h_c), the dense-packed zone’s height (h_d), and the coalescence interface height (h_c) define the boundaries of the layers. After t_i , the system stabilizes to just the dense-packed zone and distinct aqueous and organic phases. The changes in these interfaces over time are critical for understanding the separation process, which will be further explained. The next sections will detail the formulas for these stages and explore the driving mechanisms behind the interface movements and the physical processes they entail.

Based on the overall volume in a vessel as depicted in Fig. 1, the volume balance can be represented mathematically. The total volume, V_t , is the sum of the oil volume, V_o , and the water volume, V_w :

$$V_t = V_o + V_w \quad (1)$$

Given that $V_o = V_t \alpha_0$, where α_0 is the initial volume fraction of dispersed phase, we can derive the following expression for V_w :

$$V_w = V_o \left(\frac{1 - \alpha_0}{\alpha_0} \right) \quad (2)$$

Moreover, based on Fig. 4, the total volume before t_i can be broken down into the volumes of the clear light phase at the top (V_l), dense packed layer (V_d), the creaming zone (V_s), and the clear heavy phase at the bottom (V_h):

$$V_t = V_l + V_d + V_s + V_h \quad (3)$$

The volume of oil, V_o , can be expressed as:

$$\begin{aligned} V_o &= V_l + \alpha_d V_d + \alpha_0 V_s \\ V_o &= A[(H_0 - h_c) + \alpha_d(h_c - h_d) + \alpha_0(h_d - h_s)] \\ V_o &= A[H_0 - (1 - \alpha_d)h_c - (\alpha_d - \alpha_0)h_d - \alpha_0 h_s] \end{aligned} \quad (4)$$

Where H_0 , is the vessel height, A is the vessel cross-sectional, and α_d is the volume fraction of dispersed phase in dense-packed zone. In the dense-packed zone, dispersed phase droplets become more compact as they get closer together. Theoretically, the packing of hard spheres can reach a maximum value of 0.74. However, some literature reports a lower maximum packing density, around 0.65, for certain systems or under specific conditions due to droplet deformation (Henschke et al., 2002; Jeelani and Hartland, 1998). Similarly, for the water volume, V_w :

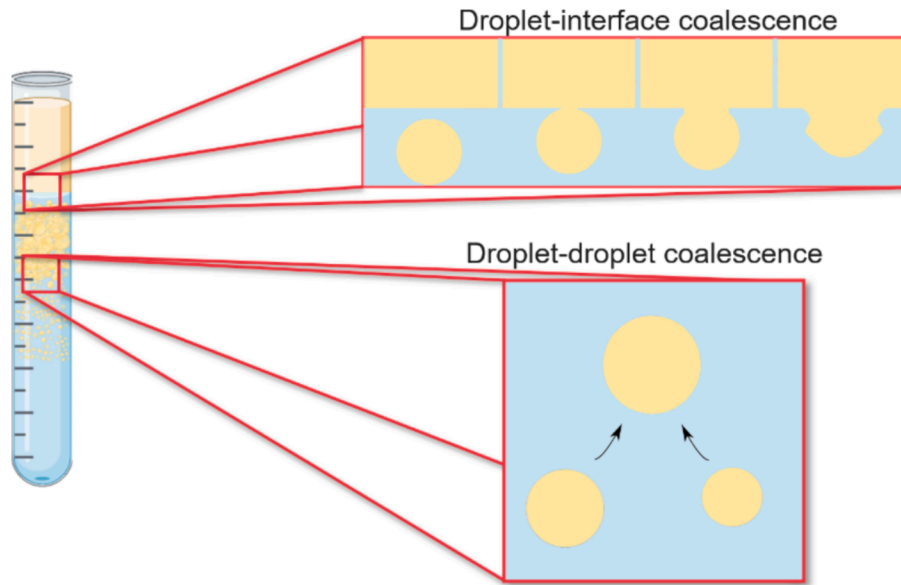


Fig. 3. Visual representation of droplet–droplet and droplet-interface coalescence processes in an emulsion, highlighting the interaction dynamics between droplets and their homophase.

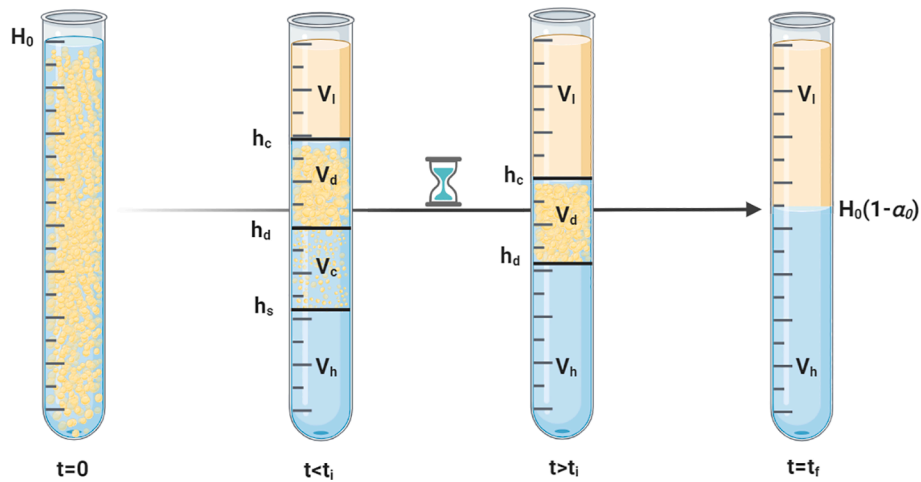


Fig. 4. The progression of layer interfaces before and after the inflection point (t_i). Represented are V_l (volume of light phase layer on top), V_d (volume of dense packed layer), V_c (volume of creaming zone), and V_h (volume of heavy phase layer at bottom).

$$V_w = (1 - \alpha_d)V_d + (1 - \alpha_0)V_s + V_h$$

$$V_w = A[(1 - \alpha_d)(h_c - h_d) + (1 - \alpha_0)(h_d - h_s) + h_s] \quad (5)$$

$$V_w = A[(1 - \alpha_d)h_c + (\alpha_d - \alpha_0)h_d + \alpha_0h_s]$$

By inserting equations (4) and (5) into equation (2), and considering that the vessel's cross-sectional area, A , is constant, we arrive at:

coalescence interface (h_c) before t_i can be determined by using the following expression:

$$\frac{dh_d}{dt} = - \left(\frac{\alpha_0}{\alpha_d - \alpha_0} \frac{dh_s}{dt} + \frac{1 - \alpha_d}{\alpha_d - \alpha_0} \frac{dh_c}{dt} \right) \quad (7)$$

Likewise, after t_i , the overall volume is made up of the clear light phase

$$\left(\frac{1 - \alpha_0}{\alpha_0} \right) (H_0 - (1 - \alpha_d)h_c - (\alpha_d - \alpha_0)h_d - \alpha_0h_s) = (1 - \alpha_d)h_c + (\alpha_d - \alpha_0)h_d + \alpha_0h_s \quad (6)$$

$$H_0 = \frac{1 - \alpha_d}{1 - \alpha_0} h_c + \frac{\alpha_d - \alpha_0}{1 - \alpha_0} h_d + \frac{\alpha_0}{1 - \alpha_0} h_s$$

By taking the time derivative of equation (6), the relation between the height of creaming zone (h_s), the dense-packed zone (h_d), and

on top (V_l), the clear water phase at the bottom (V_h), and the dense-packed zone (V_d).

$$V_t = V_l + V_d + V_h \quad (8)$$

After t_i there is no creaming zone. The dispersed phase volume fraction in the dense-packed zone (α_d) is higher than the initial volume fraction (α_0) due to the accumulation and compaction of droplets, which grow through droplet–droplet coalescence and later merge with their homophase at the interface. Then the volume of oil, V_o , can be expressed as:

$$\begin{aligned} V_o &= V_l + \alpha_d V_d \\ V_o &= A[(H_0 - h_c) + \alpha_d(h_c - h_d)] \\ V_o &= A[H_0 - (1 - \alpha_d)h_c - \alpha_d h_d] \end{aligned} \quad (9)$$

Similarly, for the water volume, V_w :

$$\begin{aligned} V_w &= (1 - \alpha_d)V_d + V_h \\ V_w &= A[(1 - \alpha_d)(h_c - h_d) + h_d] \\ V_w &= A[(1 - \alpha_d)h_c + \alpha_d h_d] \end{aligned} \quad (10)$$

When equations (9) and (10) are substituted into equation (2) and it is taken into account that the cross-sectional area of the vessel, A , remains constant, the following result is derived:

$$\begin{aligned} \left(\frac{1 - \alpha_0}{\alpha_0}\right)(H_0 - (1 - \alpha_d)h_c - \alpha_d h_d) &= (1 - \alpha_d)h_c + \alpha_d h_d \\ (1 - \alpha_0)H_0 &= (1 - \alpha_d)h_c + \alpha_d h_d \end{aligned} \quad (11)$$

By taking the time derivative of equation (11), the relation of coalescence interface and dense-packed zone height for the system can be determined by using the following expression:

$$\frac{dh_d}{dt} = -\left(\frac{1 - \alpha_d}{\alpha_d} \frac{dh_c}{dt}\right) \quad (12)$$

It was assumed that the time derivative of volume fractions (α_0 and α_d) are zero, reflecting negligible changes and rapid stabilization, in line with findings from other studies (Henschke et al., 2002; Aleem, 2021; Khan, 2019; Nadiv and Semiat, 1995; Noik et al., 2013; Aleem and Mellon, 2018; Palermo and in OTC Brasil, 2011).

Established methods exist to determine the size of gravity separators to enhance phase separation. Typically, the separator's dimensions are calculated based on the settling (or ascending) time of droplets following the principles of sedimentation for spherical particles in a Newtonian fluid at low Reynolds numbers. As Noik et al. (2013) proposed, creaming velocity can be determined by considering initial factors like volume fraction, droplet diameter and physical properties of system (Noik et al., 2013):

$$\frac{dh_s}{dt} = U_t(1 - \alpha_0)^{n_{RZ}} \left(\frac{D^2}{D_0^2}\right) \quad (13)$$

The term D^2 accounts for the impact of droplet size increase, as a result of coalescence, on their movement within the system, $(1 - \alpha_0)^{n_{RZ}}$ is a hindered settling factor and takes account of the influence of the droplet concentration in the dispersed phase on the creaming rate. The value of n_{RZ} , which falls between 2.3 and 5.5, is known as the Richardson-Zaki coefficient (Richardson, 1954). Snabre and Mills developed a comprehensive physical framework and expanded on the Richardson-Zaki formula. They introduced a variable exponent “ n ” influenced by the Reynolds number. In scenarios with a low Reynolds number, “ n_{RZ} ” approximates 5.5, whereas in denser systems, they recommend an exponent of 5.1 (Snabre and Mills, 2000). In this study $n_{RZ}=5.3$ is adopted as used in several earlier studies (Jeelani et al., 1999; Aleem, 2021; Jeelani and Hartland, 1998). D represents the droplet diameter at time (t), while D_0 represents the initial average droplet diameter. U_t is the terminal velocity and is evaluated with Stokes law as:

$$U_t = \left(\frac{\Delta\rho g D_0^2}{18\mu_c}\right) \quad (14)$$

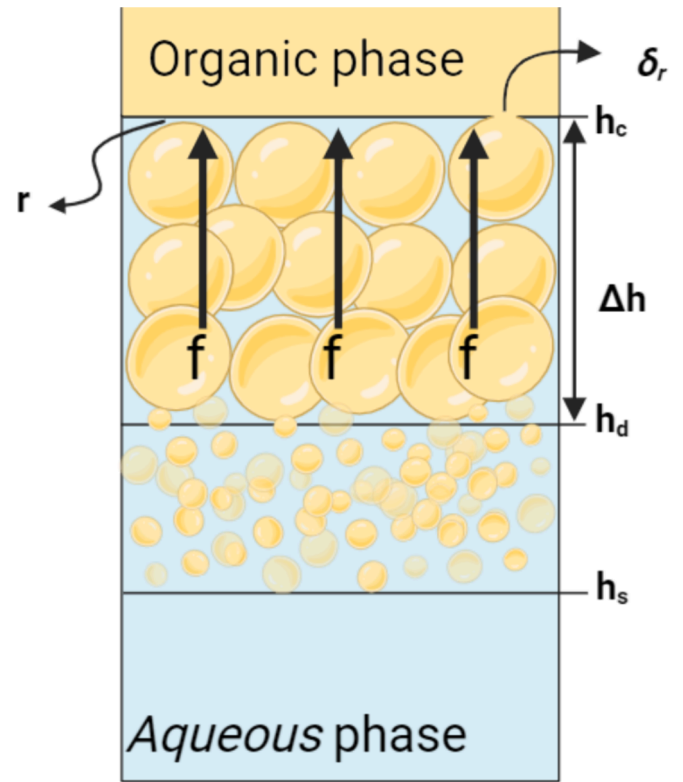


Fig. 5. Cross-sectional depiction of phase separation, showing the force (f) acting on the draining continuous phase film with radius (r) around organic phase droplets. The film's critical rupture thickness is denoted by (δ_r). The force in the dense-packed dispersion is proportional to the height difference ($\Delta h = h_c - h_d$).

$\Delta\rho$ is density difference between the dispersed and continuous phases, g is acceleration due to gravity and μ_c is dynamic viscosity of continuous phase. The terminal velocity (U_t) is multiplied by the hindered settling factor to account for the effect of adjacent droplet interactions on droplet rise velocity.

The volume rate of interfacial coalescence per unit area ($\frac{dh_c}{dt}$) is given by (Vohra and Hartland, 1978):

$$\frac{dh_c}{dt} = -\theta \frac{2\alpha_d D}{3\tau} \quad (15)$$

in which τ represents the time it takes for droplets with diameter D to coalesce with the interface. θ considers the effect of coalescence inhibition due to the presence of surfactants which will be discussed in the next section. Following Jeelani and Hartland's (1998) work, τ is inversely related to the force on the film draining over the droplet (Jeelani and Hartland, 1998). In dense-packed layer, as the Fig. 5 shows, this force relates to the height difference $\Delta h = h_c - h_d$, and for a single layer of droplets at the interface, it's related to their diameter D . The droplet-interface coalescence time is then given by:

$$\tau = \tau_0 \left(\frac{D}{D_0}\right) \left(\frac{D_0}{\Delta h}\right) \quad (16)$$

where τ_0 is the time needed for droplets of diameter D_0 in a monolayer to coalesce with the interface. τ_0 can be calculated using Jeelani and Hartland's (1994) equation (Jeelani and Hartland, 1994):

$$\tau_0 = \frac{3\pi\mu_c r^4}{4(1 + 2m)f\delta_r^2} \quad (17)$$

In Fig. 5 and Equation (16), f is the force on the draining film of the

continuous phase with radius r , while δ_r represents the film's thickness at the point of rupture. In other words, δ_r is the critical thickness at which the film breaks or ruptures. When the film radius reaches the critical thickness, it becomes unstable and ruptures. The surface mobility, m , combines the mobilities from induced circulation in nearby phases and the gradient of interfacial tension. In cases where the surface is immobile, as assumed in this work, m is set to zero.

For a drop of diameter D_0 :

$$f = \frac{\pi}{6} D_0^3 \Delta \rho g \quad (18)$$

For small droplets, the radius of the film r at an interface is equivalent to the radius of an individual droplet. The critical thickness of the film at the point of rupture, δ_r , can be determined using Vrij and Overbeek's (1968) equation (Vrij and Overbeek, 1968):

$$\delta_r = 0.267 \left(\frac{\pi r^4 A_m^2}{6 \sigma f} \right)^{\frac{1}{7}} \quad (19)$$

where σ is the interfacial tension and A_m is the Hamaker constant. The Hamaker coefficient can usually be measured experimentally, although its values for a specific system in the literature may differ by a factor of 10. However, for numerous systems, the Hamaker coefficient typically falls within the same order of magnitude (Visser, 1972). The radius of the draining film, r , can be calculated using the modified Derjaguin and Kussakov's (1939) equation for a droplet at a deformable interface (Jeelani and Hartland, 1998; Derjaguin and Kussakov, 1939):

$$r = D_0^2 \sqrt{\frac{\Delta \rho g}{12 \sigma}} \quad (20)$$

In the above equations, the evolution of droplet size due to droplet–droplet coalescence remains undefined. For the calculation of D , a population balance approach is utilized.

2.1. Population balance model for Droplet-Droplet coalescence

In this study, a population balance is applied to predict the changes in droplet size, a common method in numerous similar research (Buffo and Alopaeus, 2017; Alopaeus et al., 2007; Alopaeus et al., 2008; Alopaeus et al., 2006). The Population Balance Model (PBM) categorizes the overall droplet population and monitors their changes. This involves modeling the interactions between different sized droplets using specific closures known as kernels. For an introduction to population balances, Kumar and Ramkrishna's works from 1996 are recommended (Kumar and Ramkrishna, 1996; Kumar and Ramkrishna, 1996). In this study, the PBM is applied as a one-dimensional model, which does not account for variations in DSD at different heights within the batch settling system. The evolution of DSD is considered uniformly across the dispersed phase without spatial differentiation, focusing solely on the interactions and coalescence of droplets as categorized by their sizes. The population balance equation can then be expressed as:

$$\frac{dY_i}{dt} = B_c - D_c + S \quad (21)$$

In this context, the birth term (B_c) indicates the increase in droplet numbers within a specific category (Y_i), resulting from the merging of smaller droplets. Conversely, D_c reflects the decrease in droplet numbers in a category when droplets merged, removing them from their original size group. This process contributes to the 'death' rate of droplets in that category. Both B_c and D_c are determined by the rate of binary coalescence. The rate of binary coalescence, $r_{bc}(L_i, L_j)$, is calculated as the product of coalescence frequency (φ_c), coalescence efficiency (φ_e) and coalescence inhibition due to the presence of surfactants (θ).

$$r_{bc}(L_i, L_j) = \varphi_c(L_i, L_j) \varphi_e(L_i, L_j) \theta \quad (22)$$

L_i and L_j are the representative of i^{th} and j^{th} diameter groups, respectively. Various coalescence kernels for the rate of binary coalescence have been introduced and applied in academic research, each corresponding to different coalescing mechanisms such as those induced by shear, buoyancy, turbulence, wake entrainments, and Brownian motion (Prince and Blanch, 1990; Coualaloglou and Tavlarides, 1976; Abrahamson, 1975). In this study, we employed the Coualaloglou and Tavlarides (1976) model to calculate binary coalescence rate (Coualaloglou and Tavlarides, 1976). This model is widely used due to their straightforward formulation, although other models could also be applied without restrictions. The binary coalescence rate is determined by multiplying the droplet collision frequency (φ_c) with the collision efficiency (φ_e), leading to the subsequent formula:

$$\varphi_c(L_i, L_j) = C_1 \frac{\varepsilon}{1 + \alpha} (L_i + L_j)^2 \left(L_i^{\frac{2}{3}} + L_j^{\frac{2}{3}} \right)^{\frac{1}{2}} \quad (23)$$

$$\varphi_e(L_i, L_j) = \exp \left(-C_2 \frac{\mu_c \rho_c}{\sigma^2} \frac{\varepsilon}{(1 + \alpha)^3} \left(\frac{L_i L_j}{L_i + L_j} \right)^4 \right) \quad (24)$$

Constants C_1 and C_2 represent the model parameters as defined by Coualaloglou and Tavlarides (1976) and require calibration against empirical data. Due to the process's nature, a low turbulence energy dissipation rate (ε) is assumed. This assumption is based on the liquid–liquid decantation process relying on gravity, not external forces. As a result, the turbulence or chaotic flow within the mixture is typically low. This turbulence can arise from several factors, including the motion of the droplets (Thaker and Buwa, 2020). To address the influence of surfactants and consider the effect of coalescence inhibition due to the presence of surfactants, the following equation proposed by Håkansson et al. (2013) is used as an inhibitory factor multiplying coalescence efficiency (Håkansson, 2013):

$$\theta = \left(1 - \left(\frac{\Gamma}{\Gamma_m} \right) \right)^2 \quad (25)$$

In the equation (25) where Γ/Γ_m represents the Langmuir adsorption isotherm, this model is frequently used to describe equilibrium, particularly for non-ionic surfactants. It includes a parameter, K_L , which is the Langmuir equilibrium adsorption constant. This constant is crucial for characterizing how surfactants adhere to surfaces in equilibrium conditions.

$$\Gamma = \Gamma_m \frac{K_L c}{1 + K_L c} \quad (26)$$

Where c represents the concentration of surfactant in the bulk phase and

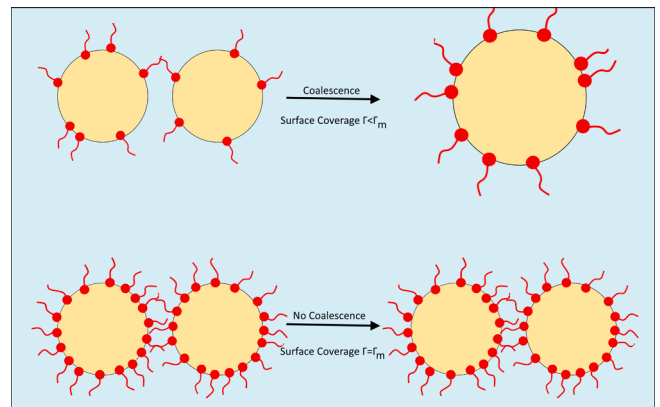


Fig. 6. Visual representation of droplet–droplet coalescence processes in an emulsion due to surfactant, highlighting the interaction dynamics between surfactant and droplet interface.

Γ_m is the maximum surface concentration. The parameter Γ_m is a theoretical limit, which is important but cannot normally be reached because of the constraint of a maximum concentration, such as the critical micelle concentration or the solubility. In this study, we assume that the surfactant is soluble only in one phase, and the mass balance is considered between the bulk phase and the droplet surface area. As depicted in Fig. 6, a large droplet surface area can adsorb surfactants, potentially leading to an insufficient amount to cover the surface. Under low surface coverage condition, this can result in droplets coalescence. However, as settling progresses and the interface area decreases, the surfactant concentration at the droplet interface increases, which can inhibit coalescence. Similar phenomenon can happen for droplet-interface coalescence.

The overall mole balance between the bulk phase and droplet interface is expressed as:

$$\frac{dn_i}{dt} = \frac{dn_{surface}}{dt} + \frac{dn_{bulk}}{dt} \quad (27)$$

In a batch system, the equation becomes:

$$\frac{dn_{surface}}{dt} + \frac{dn_{bulk}}{dt} = 0 \quad (28)$$

Since $n_{bulk} = c \times V$ and $n_{surface} = a \times \Gamma$, equation (28) leads to the following expression:

$$V_{bulk} \frac{dc}{dt} + c \frac{dV_{bulk}}{dt} + a \left(K_L \frac{\Gamma_m}{(1 + K_L c)^2} \right) \frac{dc}{dt} + \Gamma \frac{da}{dt} = 0 \quad (29)$$

Here, a is the total interfacial area of the droplets. Additionally, the change in total interfacial area is given by:

$$\frac{da}{dt} = a_i \frac{dY_i}{dt} \quad (30)$$

Where a_i is the surface area of a droplet in category i . Substituting 30 into equation (29), we get:

$$V_{bulk} \frac{dc}{dt} + c \frac{dV_{bulk}}{dt} + a \left(K_L \frac{\Gamma_m}{(1 + K_L c)^2} \right) \frac{dc}{dt} + \Gamma \sum_{i=1}^N \left(a_i \frac{dY_i}{dt} \right) = 0 \quad (31)$$

Rearranging, the equation for the change in bulk surfactant concentration over time is:

$$\frac{dc}{dt} = - \frac{c \frac{dV_{bulk}}{dt} - \Gamma \sum_{i=1}^N \left(a_i \frac{dY_i}{dt} \right)}{V_{bulk} + a \left(K_L \frac{\Gamma_m}{(1 + K_L c)^2} \right)} \quad (32)$$

The initial value of the free surfactant concentration (c_0) can be calculated by solving the following mass balance equation (Maindarkar et al., 2013):

$$c_0 = c_i - \frac{6\alpha_0}{1 - \alpha_0} \frac{\Gamma_m c_0}{c_0 + c_{1/2}} \quad (33)$$

C_i represents the concentration of surfactant used for making the emulsion, while $C_{1/2}$ is the concentration at which surfactant covers half of the maximum surface area.

Returning to equation (21), the sink term (S) is influenced by the creaming and coalescence heights in the system, as shown in Fig. 7. It represents the number of droplets removed from the population due to droplet-interface coalescence. The sink term is given by:

$$S = - \xi Y_i \quad (34)$$

Here, ξ expresses the extent of reduction in the dispersed phase volume due to interfacial coalescence, in relation to the previous time step volume.:

$$\xi = \frac{\beta'}{\beta} \quad (35)$$

In this equation, β' represents the diminishing volume fraction of the dispersion due to interfacial coalescence, indicating that the continuous phase from the dispersed layer combines with the heavy bottom layer solely when droplets coalesce with the light top layer. It is defined as follows:

$$\beta' = \frac{dh_c - dh_s}{H_0} \quad (36)$$

Phase Separation Behavior

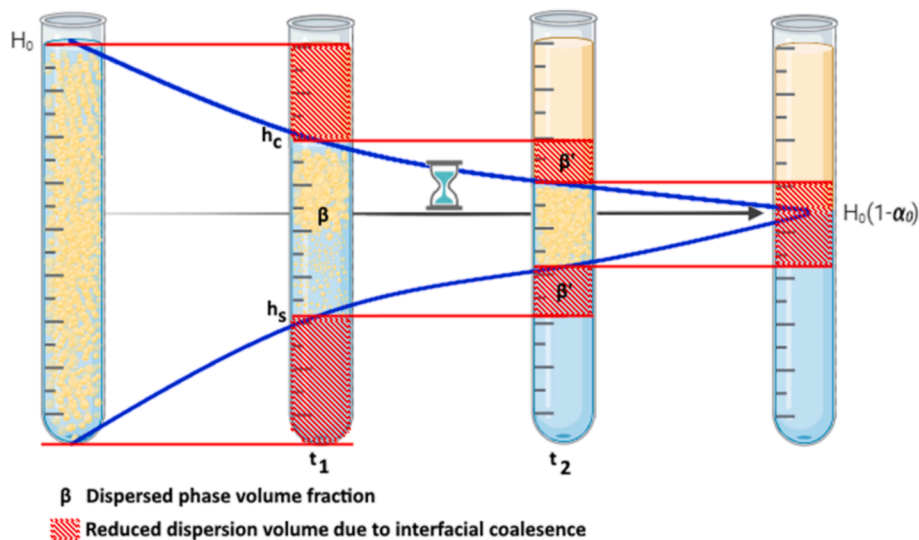


Fig. 7. Illustration of the creaming and coalescence heights within the system, demonstrating the impact of droplet-interface coalescence on the dispersion layer and the overall droplet population dynamics.

By substituting equation (36) into equation (35), we get:

$$\xi = \frac{\frac{dh_c}{dt} - \frac{dh_s}{dt}}{H_0 \beta} \quad (37)$$

And $\beta = (h_c - h_s)/H_0$. This formulation shows the dynamics of droplet removal in the system, particularly how the interfacial coalescence affects the overall droplet population.

3. Results and discussion

The proposed model's validation and sensitivity analysis are organized into three sections. Initially, the model is validated against experimental data, which serves as the base case without surfactants. The second section offers a sensitivity analysis, examining the impact of droplet size variations and preserved moments on droplet–droplet coalescence. The final section conducts another sensitivity study, exploring how surfactant concentration and Langmuir isotherm parameter (K_L) influences droplet–droplet and droplet–interface coalescence.

3.1. Model Validation, surfactant-free systems

The model is tested using two experimental datasets, focusing on liquid–liquid phase separation (Nadiv and Semiat, 1995; Jeelani and Hartland, 1998). Key parameters included the type of separation (oil in water), initial test tube height (H_0), initial droplet diameter (D_0), phase viscosities (μ) and densities (ρ), interfacial surface tension (σ), and initial dispersed phase volume fraction (α_0). Additionally, data on coalescence and creaming heights versus time were key for model validation. The first experimental dataset from Jeelani and Hartland (1998) is summarized in Table 1 and Fig. 8 (a) (Jeelani and Hartland, 1998). While this study uses data from existing literature where the impact of mixing speed is already considered, it is important to note that the influence of mixing speed is inherently accounted for in our model through the initial conditions derived from these sources. The effect of initial mixing speed on the formation of the initial volume of emulsion and droplet size distribution is acknowledged and is a critical factor as outlined in the analysis by Jeelani and Hartland (1998) (Jeelani and Hartland, 1998). While this study uses data from existing literature where the impact of mixing speed is already considered, it is important to note that the influence of mixing speed is inherently accounted for in our model through the initial conditions derived from these sources.

In the droplet coalescence model formulation, oil droplets are assumed uniformly dispersed in the water phase and initially follow a normal distribution with a specified mean diameter and standard deviation. Preliminary simulations revealed that while the system is sensitive to the initial droplet size, it remains largely insensitive to variations in the initial DSD within the discretization boundaries. This finding aligns with similar observations reported in literature, confirming the robustness of our model predictions (Chen, 2023). The mentioned

Table 1

Summary of the first set of experimental data, including Initial height of emulsion, Initial droplet diameter, Initial volume fraction of the dispersed phase. These experimental data were derived from Jeelani and Hartland (1998)^a (Jeelani and Hartland, 1998).

Parameter/ Experiment	I	II	III	IV	V	VI
H_0	0.457	0.686	0.915	0.915	0.915	0.915
D_0	847×10^{-6}	847×10^{-6}	847×10^{-6}	847×10^{-6}	680×10^{-6}	710×10^{-6}
α_0	0.3	0.3	0.3	0.4	0.5	0.6

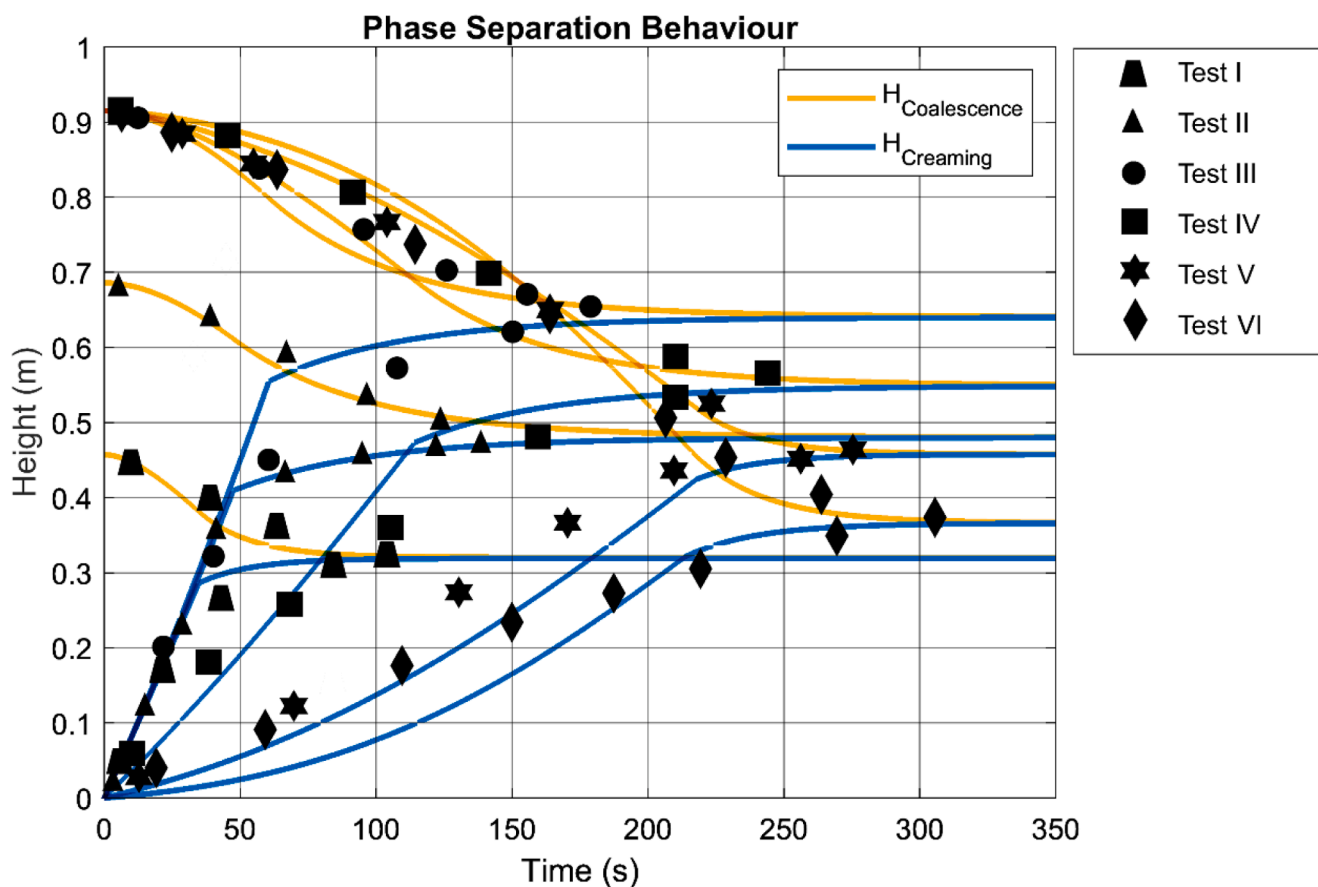
^a 25 % decane in paraffin oil mixture (density: 837.3 kg/m³, viscosity: 1.26 × 10⁻³ Pas at 20 °C) dispersed in demineralized water (density: 996 kg/m³, viscosity: 1 × 10⁻³ Pas) obtained using 25 mm diameter settler. The interfacial tension was 52.4 × 10⁻³N/m. The value of $\alpha_d = 0.65$.

experimental campaign did not include measuring the initial droplet population. As an educated guess, the initial population was assumed normal distribution and characterized by a 10 % standard deviation. This is based on the experimental study of Boxall et al. (2010) and is in accordance with the results presented in Noik et al. (2013) (Noik et al., 2013; Boxall, 2010). The estimated value of the Hamaker constant, $A_m = 8.15 \times 10^{-21}$, aligns within the same order of magnitude as values documented in related literature within the field (Aleem, 2021; Jeelani and Hartland, 1998). Once this initial distribution is formed, the population of droplets will then depend on the dispersion volume. A low dissipation rate of 0.001 (W/kg.s) was chosen due to the process's nature. The optimization technique used for fitting the Coulaloglou and Tavlirides (1976) model's constants for droplet–droplet coalescence, C_1 and C_2 , to the data from Experiment I in Table 1 aimed to minimize the mean square error (MSE) between the predicted and actual experimental outcomes. This method set the constants at $C_1 = 2 \times 10^2$ and $C_2 = 1.83 \times 10^5$.

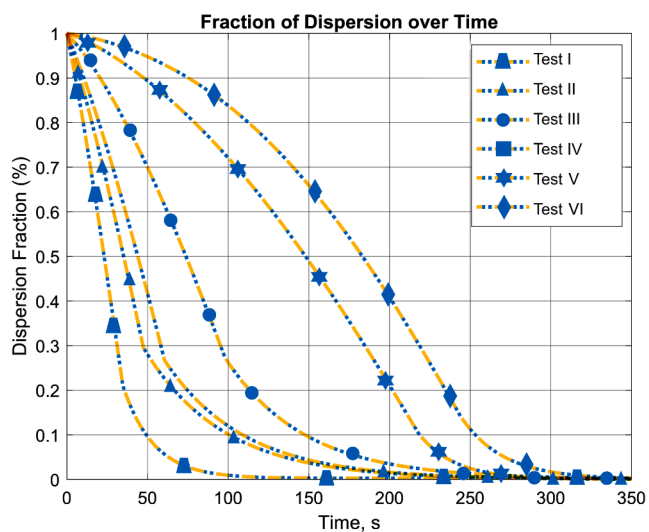
The Fig. 8 (a) presents phase separation over time, comparing the experimental results with numerical predictions. The graph shows trends in coalescence and creaming heights, marked by black dots for experimental values and continuous lines for predictions across experiment I to VI. In line with Henschke's research (Henschke et al., 2002), creaming height's trend, remains largely unchanged despite different phase ratios, suggesting minimal influence from this variable. Also, observation in coalescence height across numerical results is consistent with Jeelani and Hartland's report, noting distinct coalescence rates against constant creaming due to varying parameters. The Fig. 8 (b) shows the percentage of the dispersion fraction over time. In Tests I and II, the emulsion separates faster at first, indicated by steep initial drops. The quick separation in these tests is due to lower initial volume of the emulsion. Moving from Tests I to III, the decline is less sharp, meaning the separation starts more slowly. This slower start is linked to larger initial volumes in Tests III and VI, which show a gradual separation at the beginning. The lower rate of leveling off after inflection point, is influenced by the starting size of the droplets and the height of the mixture. Across all tests, the pattern remains consistent: an initial rapid decrease due to creaming, followed by a gradual slowdown as the separation depends on droplet–droplet and droplet–interface coalescence. The Fig. 8 (c) shows how the predicted average size of droplets increases as time passes in six tests. Although Tests I to IV share the same starting size for droplets, their differing initial conditions lead to varied final sizes. This suggests that the height and concentration of the emulsion initially can influence how much droplets grow. For Tests V and VI, which start with smaller droplets, the rate of growth and the size they reach by the end differ, indicating that the initial volume fraction has a significant impact on the coalescence process and how droplets merge over time.

The second set of experimental data is from Nadiv and Semiat (1995) and presented in Fig. 9 (a) and Table 2 (Nadiv and Semiat, 1995). The Hamaker constant value for the dataset is $A_m = 2.15 \times 10^{-21}$ (Nadiv and Semiat, 1995). The values of constants C_1 and C_2 are fitted at 6.0×10^2 and 1.7×10^5 , respectively. Fig. 9 (a), similar to Fig. 8 (a), highlights trends in coalescence and creaming heights, using black dots to denote experimental data and continuous lines for model predictions across experiments I to V. For brevity, these similar trends will not be reiterated. A key attribute of the population balance approach is its capability to track the evolution of droplet size distribution over time, as illustrated in Fig. 9 (b). This feature is particularly valuable as it allows for the direct comparison of theoretical predictions with experimental data when available.

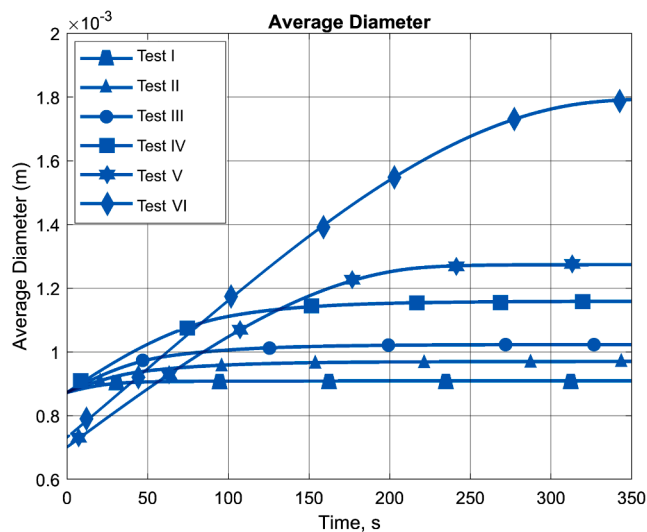
The graph in the Fig. 9 (c) illustrates the increase in average droplet diameter over time for five separate tests. Despite beginning with relatively identical droplet sizes, Tests I through IV display distinct growth patterns, implying that the initial height and volume of the emulsion significantly affect droplet enlargement. In contrast, Tests V begins with smaller droplets and shows a unique growth trajectory and final size,



(a)

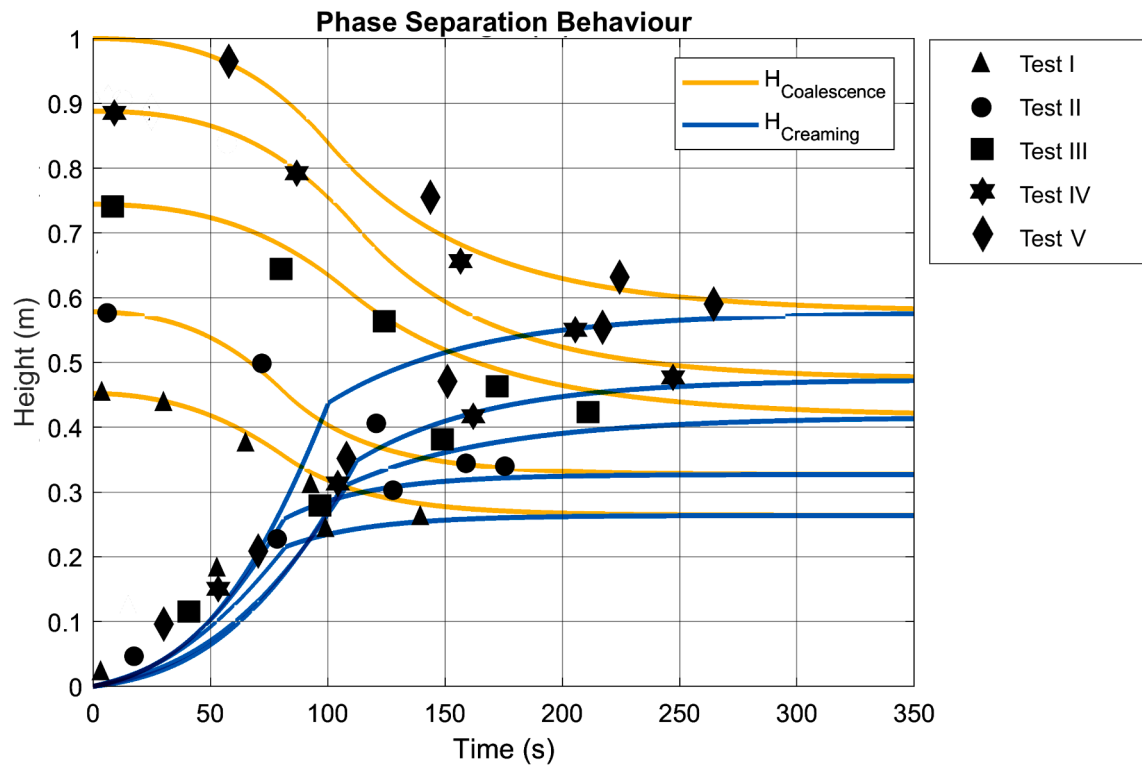


(b)

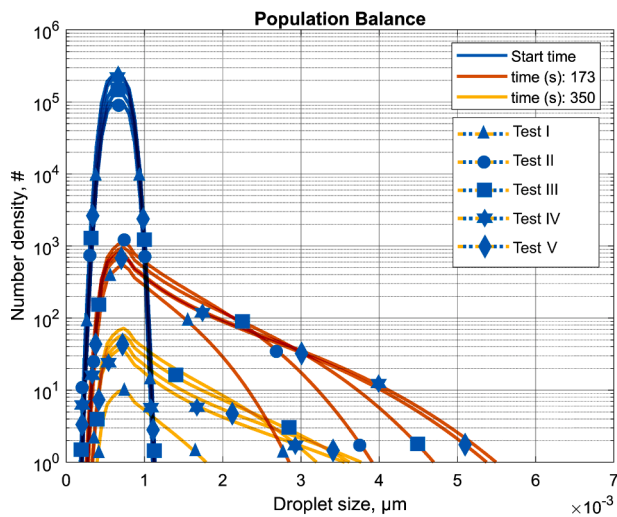


(c)

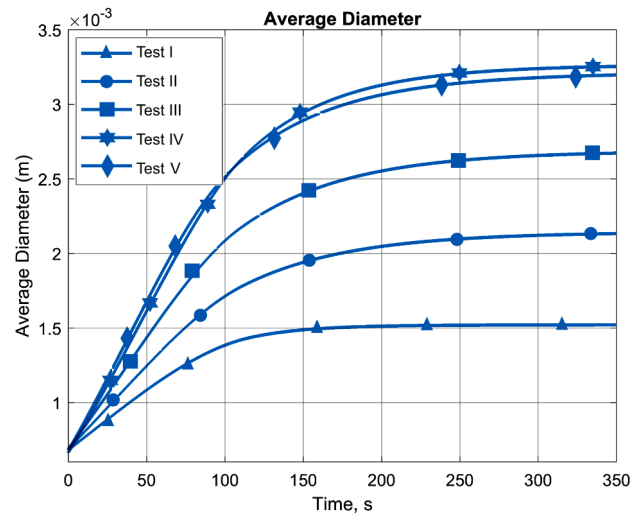
Fig. 8. (a) Comparative analysis of experimental data from Jeelani and Hartland (1998) and numerical predictions from developed model as detailed in Table 1. (b) Temporal evolution of the dispersion band volume fraction. (c) Predicted droplet size evolution based on the applied numerical model.



(a)



(b)



(c)

Fig. 9. (a) Comparative analysis of experimental data from Nadiv and Semiat (1995) and numerical predictions from developed model as detailed in Table 2. (b) Temporal evolution of the dispersion band volume fraction. (c) Predicted droplet size evolution based on the applied numerical model.

suggesting that the initial dispersed phase volume fraction markedly influences the coalescence process and the merging of droplets as time progresses.

3.2. Sensitivity analysis number of droplet size categories and preserved moments

Droplet-droplet coalescence significantly influences liquid-liquid phase separation, so this section examines how changes in the number of

droplet size groups and preserved moments affect the population balance's numerical resolution. The benchmark involves 200 groups and 6 preserved moments for the discretization method. Fig. 10 (a) and (b) presents the droplet size distribution and corresponding to Test VI of the initial experiment series.

The study explores the methodology used to examine the effects of the number of droplet size groups and preserved moments on the growth of the average droplet diameter over time. The droplet size groups were defined within a specific size range (0–5 mm) to ensure a comprehensive

Table 2

Summary of the second set of experimental data, including Initial height of emulsion, Initial droplet diameter, Initial volume fraction of the dispersed phase. These experimental data were derived Nadiv and Semiat (1995)^a (Nadiv and Semiat, 1995).

Parameter/ Experiment	I	II	III	IV	V
H_0 (m)	0.452	0.578	0.744	0.888	1.000
D_0 (m)	660×10^{-6}	670×10^{-6}	670×10^{-6}	640×10^{-6}	660×10^{-6}
α_0 (fraction)	0.416	0.434	0.440	0.466	0.422

^a 40 % n-heptane in paraffin oil (density and viscosity are 799 kg/m³ and 4.15×10^{-3} Pas) dispersed in water (density and viscosity are 998 kg/m³ and 0.98×10^{-3} Pas) obtained using a 23 mm diameter settler. The interfacial tension is 58.9×10^{-3} N/m. The temperature was about 20 °C. The value of $\alpha_d = 0.65$.

representation of the droplet population. The relative errors (difference between the average droplet size in the base case and the predicted sizes, relative to base values) are shown in Fig. 11.

The study then examines how changing the number of droplet size categories and preserved moments influences droplet population evolution (refer to Table 3 for analyzed configurations). This includes analyzing the Absolute Relative Error (ARE), which is the absolute difference between the average droplet size in the base case and the predicted sizes, relative to base values across different configurations of preserved moments and number of categories:

$$ARE = \left| \frac{D_{BaseLine} - D_{Predicted}}{D_{BaseLine}} \right| \times 100 \quad (38)$$

The selected value is the time evolution of the first moment, the mean droplet size of the population. All simulations were run for 350-seconds of physical time. For each category count and number of preserved moments, the ARE values and CPU times were assessed and are reported in Table 3. A higher ARE indicates a greater deviation from the base case, signifying less accuracy in the predictions. For instance, with 6 categories and 2 preserved moments, the ARE is 0.1631, which is much lower compared to the value of 0.9998 obtained with 200 categories and 2 preserved moments.

The solution time ratio in Table 3 shows how long it takes for the model to simulate the process in comparison to base line (119 s). As the

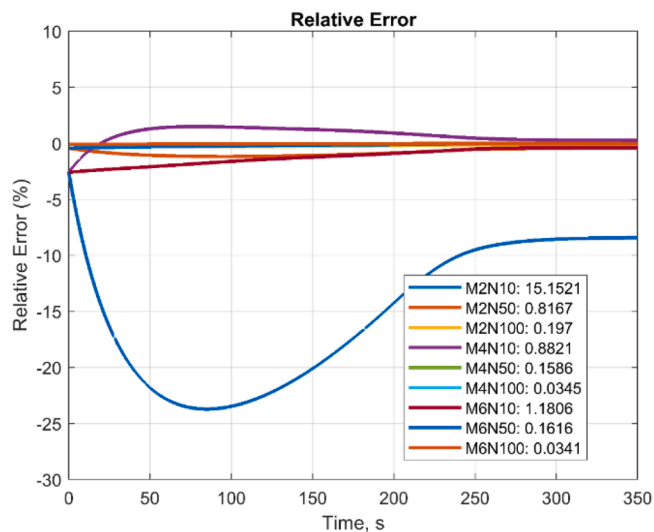
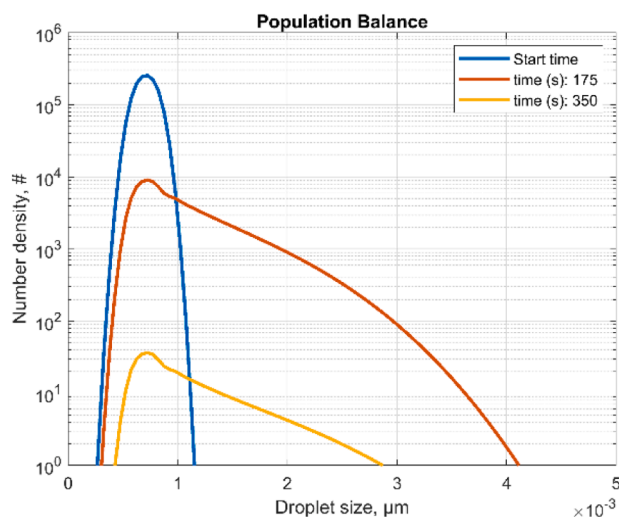


Fig. 11. Residual temporal evolution of average droplet diameter over time for varying category counts vs the reference case. The legend uses 'M' to denote the number of preserved moments and 'N' for the number of categories.

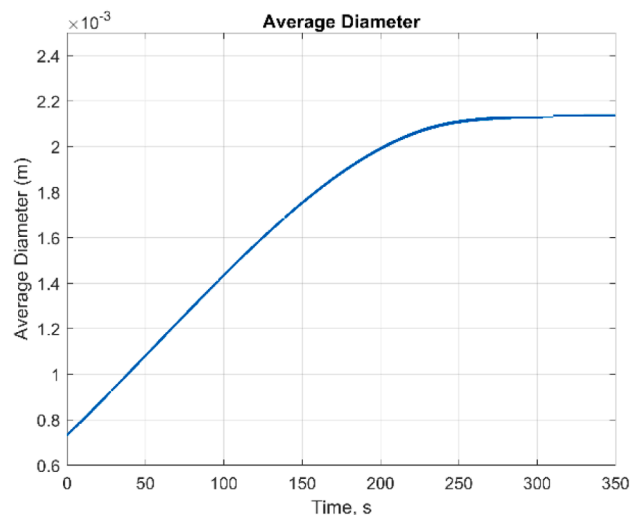
Table 3

Comparative ARE values and solution time ratio for different number of categories and preserved moments.

Number of Categories	Number of preserved moments	Average droplet size evolution case	
		ARE (%)	Solution Time Ratio ($\times 10^{-3}$)
10	2	15.15	3.28
	4	0.88	2.23
	6	1.18	3.28
50	2	0.82	4.86
	4	0.16	6.30
	6	0.16	8.93
100	2	0.20	44.77
	4	0.03	48.44
	6	0.03	56.46



(a)



(b)

Fig. 10. (a) Droplet size distribution and (b) Sauter mean diameter for the reference case with 200 droplet size categories and 6 preserved moments based on data from Test VI of first experimental dataset.

number of categories increases, the solution time increases due to the additional calculations involved, as seen in the jump from 3.28×10^{-3} with 10 categories to 4.48×10^{-2} with 100 categories when preserving 2 moments.

Based on the obtained results, 100 categories and 4 moments were used throughout this paper. We considered that this is a reasonable compromise between the effect of the numerical discretization and the simulation time.

3.3. Effect of surfactant concentration and Langmuir isotherm parameter

Surfactants play a key role in droplet coalescence, significantly influencing the process due to their amphiphilic nature. They adsorb at the droplet interface and can substantially change coalescence dynamics, with their concentration and strength being key factors. The following sections present results from two hypothetical scenarios, exploring the effects of different surfactant concentrations and Langmuir parameter in the model. These hypothetical scenarios help illustrate the framework for incorporating surfactant effects into the model, without specifying particular surfactants, and demonstrate the model's potential applications. The findings, based on hypothetical data, are interpreted in line with established scientific literature for consistency with known principles. The analysis is divided into two parts: firstly, examining the effects of surfactant concentration changes, and secondly, assessing the impact of Langmuir Isotherm Parameter (K_L) on the process.

3.3.1. Surfactant concentration

This section examines how different surfactant concentrations affect liquid–liquid phase separation, offering insights into the mechanisms and empirical support for the observed phenomena. The study tests surfactant concentrations of 0 (control, surfactant free system), 1×10^{-1} , 2×10^{-1} , and 3×10^{-1} mol/m³, observing the resulting changes in droplet coalescence. All simulations maintained consistent initial conditions: K_L at 100 m³/mol (corresponding to a moderate surfactant (Chang and Franses, 1995), Γ_m at 4×10^{-3} mol/m², a mean droplet diameter of 110 μ m, an emulsion height of 915 mm, and an initial dispersed phase volume fraction (α_0) of 0.3, alongside other fluid properties from Jeelani and Hartland (1998) dataset in Section 3.1.

Fig. 12 illustrates the influence of surfactant concentration on phase separation and droplet behavior. With increasing surfactant levels, the time for phase separation lengthens, highlighting the stabilizing effect of surfactants. For instance, As the Fig. 12 (a) shows, a moderate increase in concentration leads to a noticeable extension in separation time. High surfactant levels result in significant surface coverage, effectively preventing droplet coalescence and maintaining uniform dispersion, as depicted in Fig. 12 (b). Without surfactants, phase separation is swift, occurring in a much shorter period. The model is capable of simulating a stable emulsion, particularly when surfactants achieve maximum surface coverage (e.g., $\Gamma/\Gamma_m > 95\%$), effectively halting droplet–interface coalescence, as demonstrated with a surfactant concentration of 3×10^{-1} mol/m³. The impact on droplet sizes is also marked in Fig. 12 (c); higher

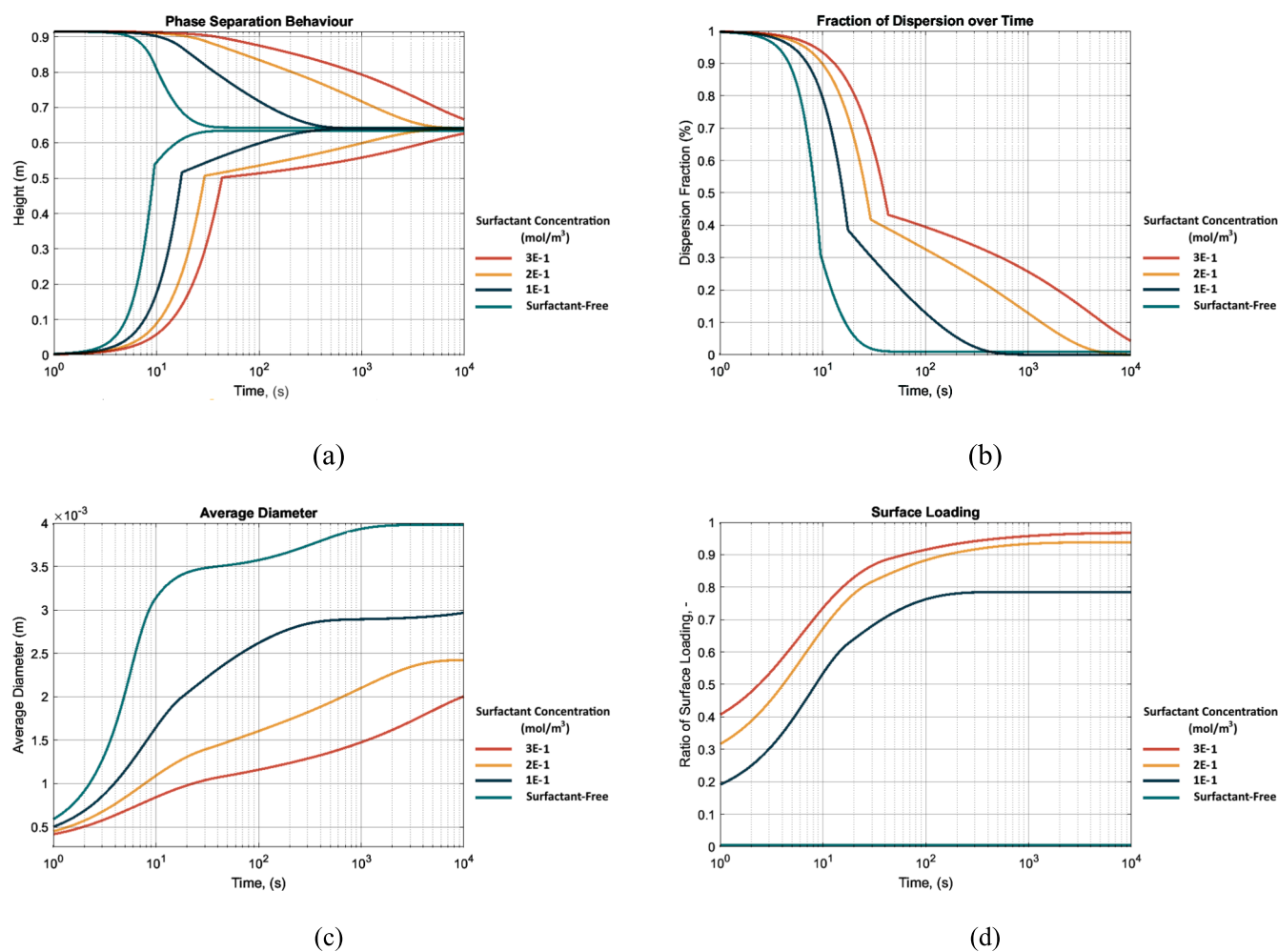


Fig. 12. Depiction of liquid–liquid phase separation behavior and coalescence dynamics at varying surfactant concentrations (free-surfactant, 1×10^{-1} , 2×10^{-1} , and 3×10^{-1} mol/m³). (a) Phase separation time plotted against surfactant concentration. (b) Dispersion band behavior over time across surfactant concentration. (c) Mean droplet size evolution. (d) Surface loading.

concentrations result in smaller droplet sizes due to increased surfactant presence at the interface, which enhances repulsive forces against droplet coalescence. In contrast, the absence of surfactants sees considerably larger maximum droplet diameters. As surfactant concentration grows, the observed maximum droplet sizes decrease, indicating restricted droplet growth and enhanced stability.

Fig. 12 (d) demonstrates that at lower concentrations, insufficient surfactant particles lead to minimal surface coverage, reducing repulsion and facilitating larger droplet formation. Increasing the surfactant concentration improves surface coverage, creating a barrier that significantly prevents droplets from coalescing. At high concentrations, surface coverage nears completion, maximizing droplet stabilization and minimizing coalescence. This behavior aligns with the Langmuir isotherm, suggesting surfactant coverage on droplets increases with concentration until saturation, providing a protective layer against droplet–droplet coalescing.

3.3.2. Langmuir parameter

The effectiveness of surfactant can also be gauged by its Langmuir constant K_L , dictating its ability to stabilize emulsions. To discern the effects of varying surfactant types, three hypothetical surfactants are analyzed, denoted by their K_L values as weak ($100 \text{ m}^3/\text{mol}$), moderate ($500 \text{ m}^3/\text{mol}$), and strong ($1000 \text{ m}^3/\text{mol}$), according to classifications established by Chang and Franses (1995) (Chang and Franses, 1995). For the purpose of this analysis, a consistent surfactant concentration of

$1 \times 10^{-1} \text{ mol}/\text{m}^3$ and maximum surface concentration (Γ_m) of $4 \times 10^{-3} \text{ mol}/\text{m}^2$ was maintained, while other system properties are aligned with those discussed in section 3.3.1.

Fig. 13 (a) clearly shows how phase separation time is influenced by surfactant type. A weaker surfactant leads to faster separation, indicating low resistance to coalescence. As surfactant strength increases, so does the resistance, resulting in longer separation times for moderate and strong surfactants. With a weak surfactant, phase separation occurs in less time, whereas a moderate surfactant extends this to twice. At $K_L=1000$, the surfactant achieves over 95 % surface coverage, stopping creaming and coalescence (Fig. 13 (b)). Fig. 13 (c) reveals how droplet size is affected by surfactant type. Weak surfactants allow for larger droplets due to less effective resistance, while moderate and strong surfactants result in smaller, more stable droplets. The figure also highlights the relationship between surfactant strength and maximum mean droplet size. Stronger surfactants lead to smaller droplet sizes; for instance, droplets average $450 \mu\text{m}$ with a weak surfactant but reduce to $145 \mu\text{m}$ with a strong one. This size reduction from weak to strong surfactants underscores the reduced coalescence. Additionally, the time taken for droplets to reach their peak size varies with surfactant strength. These findings confirm the significant impact of surfactant type on coalescence dynamics.

The Fig. 13 (d) demonstrates the impact of surfactant type on surface loading. A weak surfactant ($100 \text{ m}^3/\text{mol}$) results in insufficient molecules to cover the droplets interface, leading to easier coalescence. As

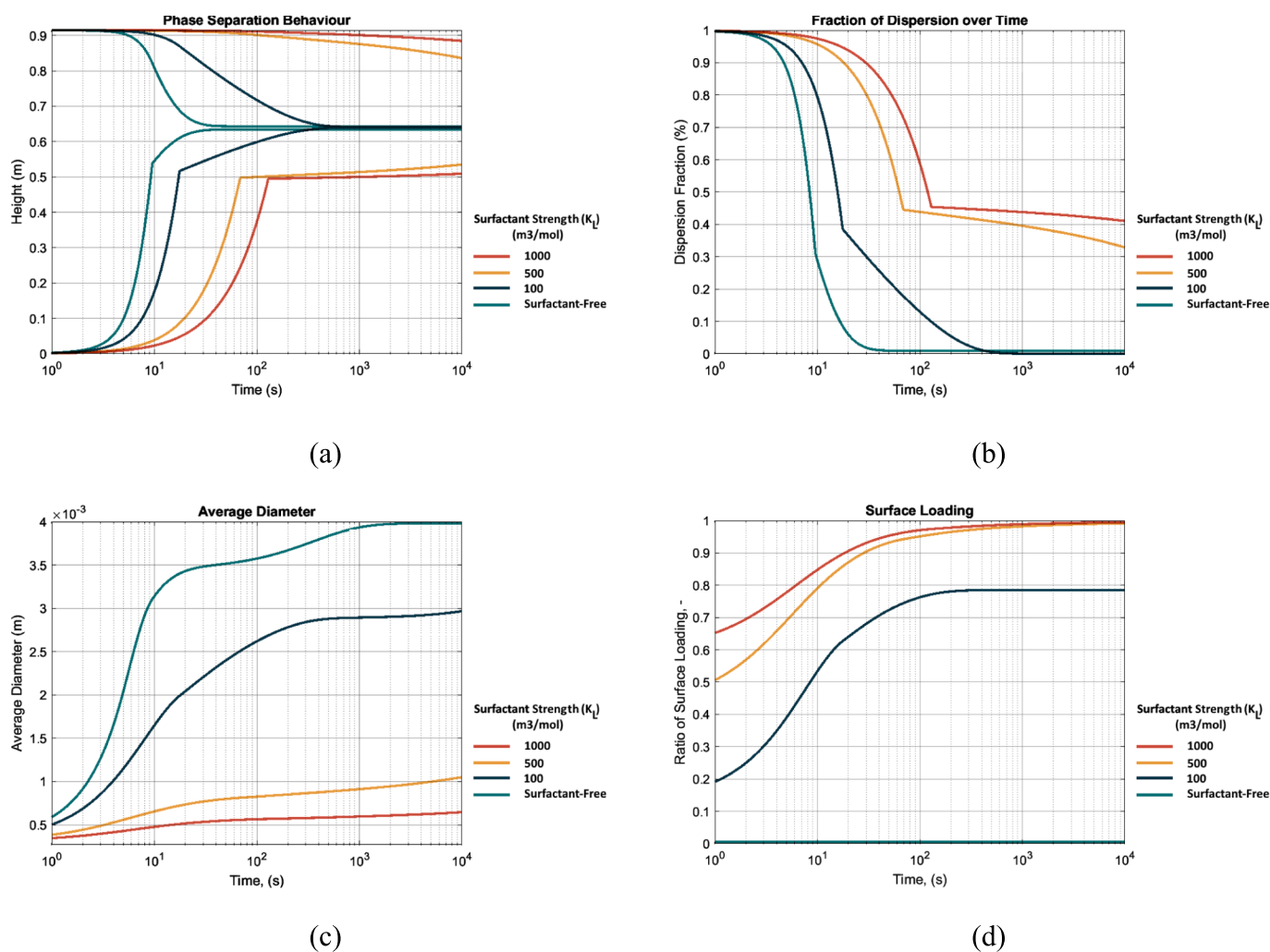


Fig. 13. Comparative analysis of surfactant type (surfactant-free, 100, 500, $1000 \text{ m}^3/\text{mol}$) on liquid–liquid phase separation dynamics. (a) Phase separation time plotted against surfactant type. (b) Dispersion band behavior over time across surfactant type. (c) Mean droplet size evolution. (d) Surface loading.

surfactant strength increases (500 and 1000 m³/mol), droplets become more stable, with surface loading nearing 0.95, signifying nearly complete coverage that maintains droplet separation. In contrast, a system without surfactant shows quick phase separation and much higher average droplet diameter. These trends are consistent with the Langmuir isotherm, which suggests surfactant molecules will increasingly cover droplet surfaces with higher concentrations until a full layer is formed, preventing coalescence.

4. Conclusion

The present model provides a framework for understanding the dynamics of liquid–liquid phase separation, specifically the influence of surfactants on droplet–droplet and droplet–interface coalescence. Initial validation against established experimental data confirms the model's reliability in scenarios without surfactants. The further sensitivity analyses clarify the effect of system properties and surfactant levels. The analyses show the model's ability to react to changes in surfactant concentration, proving it can generate results that agree with physical laws. The results highlight the stabilizing effect of surfactants, demonstrating that increased concentrations lead to reduced droplet coalescence and smaller droplet sizes, thereby extending the time required for phase separation. Higher concentrations of surfactants lead to higher coverage on droplet surfaces, increasing repulsion between droplets and thus preventing coalescence. The model incorporates surfactant concentrations and their effectiveness using appropriate isotherms, allowing for the prediction of hindered settling behavior. Literature on applying population balance approaches to predict drop size distribution evolution is limited, which our model addresses as a contribution to the field. These results provide guidance for enhancing the design of large-scale decanters and the stability of emulsions in industrial settings by fine-tuning the system properties.

CRedit authorship contribution statement

Mahdi Mousavi: Writing – review & editing, Writing – original draft, Visualization, Validation, Software, Methodology, Conceptualization. **Andreu Bernad:** Writing – review & editing, Software, Methodology, Conceptualization. **Ville Alopaeus:** Writing – review & editing, Supervision, Funding acquisition, Conceptualization.

Declaration of competing interest

The authors declare that they have no known competing financial interests or personal relationships that could have appeared to influence the work reported in this paper.

Data availability

Data will be made available on request.

Acknowledgement

This work was supported by Neste Oyj, Finland. Many thanks to Dr. Lena Hohl for her invaluable feedback and guidance throughout.

References

- Abrahamson, J., 1975. Collision rates of small particles in a vigorously turbulent fluid. *Chem. Eng. Sci.* 30 (11), 1371–1379.
- Ahmad, J. and L.M. Nollet, *Nanoemulsions in Food Technology: Development, Characterization, and Applications*. 2021: CRC Press.
- Aleem, W., et al., 2021. Experimental investigation and mathematical modeling of oil/water emulsion separation effectiveness containing alkali-surfactant-polymer. *J. Dispers. Sci. Technol.* 42 (9), 1286–1298.
- Aleem, W., Mellon, N., 2018. Model for the prediction of separation profile of oil-in-water emulsion. *J. Dispers. Sci. Technol.* 39 (1), 8–17.
- Alopaeus, V., 2022. Modeling surfactant and drop size dynamics in polydisperse liquid–liquid systems with population balances. *Chem. Eng. Sci.* 248, 117269.
- Alopaeus, V., Laakkonen, M., Aittamaa, J., 2006. Solution of population balances with breakage and agglomeration by high-order moment-conserving method of classes. *Chem. Eng. Sci.* 61 (20), 6732–6752.
- Alopaeus, V., Laakkonen, M., Aittamaa, J., 2007. Solution of population balances with growth and nucleation by high order moment-conserving method of classes. *Chem. Eng. Sci.* 62 (8), 2277–2289.
- Alopaeus, V., Laakkonen, M., Aittamaa, J., 2008. Solution of population balances by high order moment-conserving method of classes: reconstruction of a non-negative density distribution. *Chem. Eng. Sci.* 63 (10), 2741–2751.
- Bhardwaj, A., Hartland, S., 1994. Kinetics of coalescence of water droplets in water-in-crude oil emulsions. *Journal of Dispersion Science And Technology* 15 (2), 133–146.
- Boxall, J.A., et al., 2010. Measurement and calibration of droplet size distributions in water-in-oil emulsions by particle video microscope and a focused beam reflectance method. *Ind. Eng. Chem. Res.* 49 (3), 1412–1418.
- Buffo, A., Alopaeus, V., 2017. A novel simplified multivariate PBE solution method for mass transfer problems. *Chem. Eng. Sci.* 172, 463–475.
- Chang, C.-H., Franses, E.I., 1995. Adsorption dynamics of surfactants at the air/water interface: a critical review of mathematical models, data, and mechanisms. *Colloids Surf A Physicochem Eng Asp* 100, 1–45.
- Chen, J., et al., 2023. Computational fluid dynamics simulations of phase separation in dispersed oil-water pipe flows. *Chem. Eng. Sci.* 267, 118310.
- Coulaloglou, C., Tavlarides, L.L., 1976. Drop size distributions and coalescence frequencies of liquid-liquid dispersions in flow vessels. *AIChE J* 22 (2), 289–297.
- Cunha, R.E., et al., 2008. Mathematical modeling of the destabilization of crude oil emulsions using population balance equation. *Ind. Eng. Chem. Res.* 47 (18), 7094–7103.
- Deng, S., et al., 2002. Effects of alkaline/surfactant/polymer on stability of oil droplets in produced water from ASP flooding. *Colloids Surf A Physicochem Eng Asp* 211 (2–3), 275–284.
- Derjaguin, B., Kussakov, M., 1939. Anomalous properties of thin polymolecular films. *Acta Physicochim. URSS* 10 (1), 25–44.
- Gomes, E.F., Guimarães, M., Ribeiro, L.M., 2007. Numerical modelling of a gravity settler in dynamic conditions. *Adv. Eng. Softw.* 38 (11–12), 810–817.
- Grimes, B., 2012. Population balance model for batch gravity separation of crude oil and water emulsions. Part I: model formulation. *J. Dispers. Sci. Technol.* 33 (4), 578–590.
- Haegel, F.H., et al., 2009. *Microemulsions in Large-Scale Applications*. Microemulsions: Background, New Concepts, Applications. Perspectives 302–344.
- Håkansson, A., et al., 2013. A high-pressure homogenization emulsification model—Improved emulsifier transport and hydrodynamic coupling. *Chem. Eng. Sci.* 91, 44–53.
- Hassanpour, S., et al., 2018. On the impact of Co3O4 nanoparticles on interaction of heavy oil and brine mixtures. *J. Pet. Sci. Eng.* 171, 680–686.
- Henschke, M., Schlieper, L.H., Pfennig, A., 2002. Determination of a coalescence parameter from batch-settling experiments. *Chem. Eng. J.* 85 (2–3), 369–378.
- Hidayah, N.N., Abidin, S.Z., 2018. The evolution of mineral processing in extraction of rare earth elements using liquid-liquid extraction: A review. *Miner. Eng.* 121, 146–157.
- Hooper, W., Jacobs Jr, L., Decantation, 1979. *Handbook of Separation Methods for Chemical Engineers*. McGraw-Hill, New York.
- Jeelani, S.A.K., Hartland, S., 1986. Prediction of dispersion height in liquid-liquid gravity settlers from batch settling data. *Chem. Eng. Res. Des.* 64 (6), 450–460.
- Jeelani, S., Hartland, S., 1994. Effect of interfacial mobility on thin film drainage. *J. Colloid Interface Sci.* 164 (2), 296–308.
- Jeelani, S.A.K., Hartland, S., 1998. Effect of dispersion properties on the separation of batch liquid–liquid dispersions. *Industrial & Engineering Chemistry Research* 37 (2), 547–554.
- Jeelani, S., Panoussopoulos, K., Hartland, S., 1999. Effect of turbulence on the separation of liquid–liquid dispersions in batch settlers of different geometries. *Ind. Eng. Chem. Res.* 38 (2), 493–501.
- Khan, J.A., et al., 2019. Influence of alkali-surfactant-polymer flooding on the coalescence and sedimentation of oil/water emulsion in gravity separation. *J. Pet. Sci. Eng.* 173, 640–649.
- Kumar, S., Ramkrishna, D., 1996. On the solution of population balance equations by discretization—I. A fixed pivot technique. *Chem. Eng. Sci.* 51 (8), 1311–1332.
- Kumar, S., Ramkrishna, D., 1996. On the solution of population balance equations by discretization—II. A moving pivot technique. *Chem. Eng. Sci.* 51 (8), 1333–1342.
- Maindarkar, S.N., Bongers, P., Henson, M.A., 2013. Predicting the effects of surfactant coverage on drop size distributions of homogenized emulsions. *Chem. Eng. Sci.* 89, 102–114.
- Mousavi, S.M., Sadeghnejad, S., Ostadhassan, M., 2021. Evaluation of 3D printed microfluidic networks to study fluid flow in rocks. *Oil & Gas Science and Technology-Revue d'IFP Energies Nouvelles* 76, 50.
- Nadiv, C., Semiat, R., 1995. Batch settling of liquid-liquid dispersion. *Ind. Eng. Chem. Res.* 34 (7), 2427–2435.
- Noik, C., Palermo, T., Dalmazzone, C., 2013. Modeling of liquid/liquid phase separation: Application to petroleum emulsions. *J. Dispers. Sci. Technol.* 34 (8), 1029–1042.
- Palermo, T., et al., 2011. Liquid-Liquid Separation in Gravitational Subsea Separators. *OnePetro*.
- Prince, M.J., Blanch, H.W., 1990. Bubble coalescence and break-up in air-sparged bubble columns. *AIChE J* 36 (10), 1485–1499.
- Richardson, J.T., 1954. Sedimentation and fluidization: Part I. *Trans. Inst. Chem. Engrs.* 32, 35–52.

- Ruiz, M., Padilla, R., 1996. Separation of liquid-liquid dispersions in a deep-layer gravity settler: Part II: Part II. Mathematical modeling of the settler. *Hydrometallurgy* 42 (2), 281–291.
- Schneider, D.R., Aris, R., Amundson, N.R., 1973. An analysis of chemical reactor stability and sensitivity—XIV the effect of the steady state hypothesis. *Chem. Eng. Sci.* 28 (3), 885–896.
- Snabre, P., Mills, P., 2000. Settling and fluidization of non Brownian hard spheres in a viscous liquid. *The European Physical Journal E* 1, 105–114.
- Stewart, M. and K. Arnold, *Gas-liquid and Liquid-liquid Separators*. 2008: Gulf Professional Publishing.
- Stokes, G.G., *On the effect of the internal friction of fluids on the motion of pendulums*. 1851.
- Thaker, A.H., Buwa, V.V., 2019. Experimental investigations of interfacial and binary coalescence of multilayered drops. *Ind. Eng. Chem. Res.* 58 (18), 7620–7632.
- Thaker, A.H., Buwa, V.V., 2020. Separation of liquid-liquid dispersion in a batch settler: CFD-PBM simulations incorporating interfacial coalescence. *AIChE J* 66 (11), e16983.
- Visser, J., 1972. On Hamaker constants: A comparison between Hamaker constants and Lifshitz-van der Waals constants. *Adv. Colloid Interface Sci.* 3 (4), 331–363.
- Vohra, D., Hartland, S., 1978. Shape of a vertical column of drops approaching an interface. *AIChE Journal* 24 (5), 811–817.
- Vrij, A., Overbeek, J.T.G., 1968. Rupture of thin liquid films due to spontaneous fluctuations in thickness. *J. Am. Chem. Soc.* 90 (12), 3074–3078.
- Wang, Z., Bai, Y., Zhao, X., 2012. Study on emulsification properties of ethanalamine and sodium carbonate. *Applied Chemical Industry* 41 (4), 566–569.
- Wang, H., Davis, R.H., 1995. Simultaneous sedimentation and coalescence of a dilute dispersion of small drops. *J. Fluid Mech.* 295, 247–261.